The Astrophysical Journal, 704:L85–L88, 2009 October 20 doi:10.1088/0004-637X/704/2/L85
© 2009. The American Astronomical Society. All rights reserved. Printed in the U.S.A.

INTERACTIONS OF THE MAGNETOSPHERES OF STARS AND CLOSE-IN GIANT PLANETS

O. Cohen[1], J. J. Drake[1], V. L. Kashyap[1], S. H. Saar[1], I. V. Sokolov[2], W. B. Manchester IV[2], K. C. Hansen[2], and T. I. Gombosi[2]
[1] Harvard-Smithsonian Center for Astrophysics, 60 Garden St., Cambridge, MA 02138, USA
[2] Center for Space Environment Modeling, University of Michigan, 2455 Hayward St., Ann Arbor, MI 48109, USA
Received 2009 July 13; accepted 2009 September 15; published 2009 September 30

ABSTRACT

Since the first discovery of an extrasolar planetary system more than a decade ago, hundreds more have been discovered. Surprisingly, many of these systems harbor Jupiter-class gas giants located close to the central star, at distances of 0.1 AU or less. Observations of chromospheric "hot spots" that rotate in phase with the planetary orbit, and elevated stellar X-ray luminosities, suggest that these close-in planets significantly affect the structure of the outer atmosphere of the star through interactions between the stellar magnetic field and the planetary magnetosphere. Here, we carry out the first detailed three-dimensional magnetohydrodynamics simulation containing the two magnetic bodies and explore the consequences of such interactions on the steady-state coronal structure. The simulations reproduce the observable features of (1) increase in the total X-ray luminosity, (2) appearance of coronal hot spots, and (3) phase shift of these spots with respect to the direction of the planet. The proximate cause of these is an increase in the density of coronal plasma in the direction of the planet, which prevents the corona from expanding and leaking away this plasma via a stellar wind. The simulations produce significant low temperature heating. By including dynamical effects, such as the planetary orbital motion, the simulation should better reproduce the observed coronal heating.

Key words: planetary systems – stars: coronae

1. INTRODUCTION

The structure and heating of the solar corona, as well as the acceleration of the solar wind, are influenced by the structure and topology of the large-scale coronal magnetic field. On this basis, the existence of a planet at a distance of 0.1 AU or less (Mayor & Queloz 1995; Mayor et al. 2003), with a strong internal magnetic field is expected to have a significant effect on the stellar magnetosphere, which is controlled by the magnetic field structure (Cuntz et al. 2000). In recent years, some signatures of this star–planet interaction (SPI) have been observed. Shkolnik et al. (Shkolnik et al. 2003, 2005a, 2005b, 2008) have reported on modulations in the Ca II K emission line, an indicator for chromospheric activity. They find enhancements in the line intensity that have the same period as the planetary orbital motion, though sometimes with a significant non-zero phase shift. The cause is deemed magnetic and not tidal because of the lack of an equivalent hot spot offset in phase by 180°. In addition, a statistical survey of the X-ray fluxes from stars with close-in planets has found them enhanced by 30%–40% on average over typical fluxes from similar stars with planets that are not close-in (Kashyap et al. 2008). Direct X-ray observations of the HD 179949 system (Saar et al. 2008) showed that the SPI contributed ≈30% to the emission at a mean temperature of ≈1 keV.

Some analytical and semiempirical arguments have been advanced to explain these observations. One posits that particles are accelerated along magnetic field lines that connect the star and planet, creating hot spots where they hit the chromospheric layer (Cuntz et al. 2000; Lanza 2008; Cranmer & Saar 2007). As a result, hot spots are observed generally in phase with the planetary orbit, but with the capacity to have large offsets, depending on the exact structure of the magnetic field between the star and the planet. Another shows that transition of field lines from a high-helicity state to a linear force-free state is energetically adequate to power the enhanced intensities (Lanza 2009). The detailed behavior of the dynamical interaction of coronal and wind plasma with two magnetic field systems is, however, very difficult to realize with idealized models. The problem properly requires simultaneous descriptions of both the stellar and the planetary magnetospheres, the planetary orbital motion, and often asynchronous stellar rotation, together with a self-consistent stellar wind solution.

Here, we describe an initial simulation of the magnetic SPI. We use idealized test cases to study the fundamental changes in the steady-state coronal structure due to the presence of the planet and its magnetic field. The dynamical interaction due to the planetary orbital motion is captured in an indirect manner.

2. SIMULATION

The numerical simulation has been performed using the University of Michigan Solar Corona (SC) model (Cohen et al. 2007), which is based on the BATS-R-US global magnetohydrodynamics (MHD) code (Powell et al. 1999) and is part of the Space Weather Modeling Framework (SWMF; Tóth et al. 2005). The model solves the set of magnetohydrodynamic equations on a Cartesian grid using adaptive mesh refinement (AMR) technology. This model has been extensively validated for the solar corona using coronal observations and in situ solar wind measurements taken at 1 AU (Cohen et al. 2008). We assume that the particular physical description of the coronal heating and wind acceleration is not crucial for studying the change in the existing coronal structure due to the planet. It is important to mention that we use a *global* model for the corona that cannot reproduce realistic chromospheric emission due to heating of coronal loops. We also do not fully describe the observed coronal heating, since, for example, no input from magnetic reconnection or loop footpoint motion is included. Thus, while we adopt the physical parameters of some real systems in the modeling, we do not expect the models to fully reproduce all aspects of observations (in particular, details of the temperature

and level of the emissions) at this point. The full physical description of the model and its limitations can be found in Cohen et al. (2007, 2008).

We performed several different numerical simulations, of which we highlight two here. "Case A": both the stellar and planetary magnetic fields are perfectly aligned dipoles. We set the stellar polar field to be 5 G and the planetary polar field to be antiparallel at −2 G (i.e., opposite to the stellar dipole). The planetary magnetic field is weaker than Jupiter's, and follows the assumption that hot Jupiters are expected (but not required) to have lower spin rates due to tidal locking, and thus have weaker magnetic fields (Sánchez-Lavega 2004; Grießmeier et al. 2004; Olson & Christensen 2006). We note that a simulation in which the planetary dipole was set to be in the same direction with the stellar dipole resulted in a quantitatively similar solution as in this case. "Case B": the planetary magnetic field is a perfect dipole and the stellar magnetic field is driven by solar magnetic synoptic map (magnetogram). This map contains measurements of the photospheric radial magnetic field taken during solar maximum (Carrington Rotation CR2010, very active Sun). The use of a magnetic synoptic map enables us to generate a realistic, Sun-like, three-dimensional magnetic field.

In Case A, we mimic the relative motion between the planet and the background plasma by fixing the planet and rotating the star and the coronal plasma in the inertial frame. This way, the planet orbits the star backward in the frame rotating with the star. This is done due to the fact that the actual orbital motion of the planet requires time-dependent boundary conditions. We plan to implement this technical improvement in future simulations. For the sake of definiteness, we partially match the parameters of the system to the observed parameters of HD 179949 (Mayor et al. 2003), which is an F8V type star. We use the following stellar parameters: $M_\star = 1.28\ M_\odot$, $R_\star = 1.19\ R_\odot$, and stellar rotation period of 3d. In the HD 179949 system, the planet is located at a distance of 0.045 AU (9.65 stellar radii), and a 60° phase lead of a chromospheric hot spot is observed. The planetary parameter $M \sin i = 0.98\ M_J$ has not been used here. In Case B, we fix the planet relative to the star and run the simulation in the frame rotating with the star. In this case, we use solar parameters except for the planetary properties, which are the same as in Case A. This case represents a steady-state, large-scale interaction of a Sun-like star with a tidally locked extrasolar planet (e.g., τ Boo; Saar et al. 2004; Catala et al. 2007) located at the same distance as before.

In both simulations, the boundary condition for the planetary plasma number density and temperature were $n_0 = 10^{10}$ cm^{-3} and $T_0 = 10^4$ K, respectively (Murray-Clay et al. 2009). The stellar boundary conditions were $n_0 = 10^9$ cm^{-3} and $T_0 = 3.5 \times 10^6$ K, respectively, based on previous simulation of the solar corona (Cohen et al. 2007). To further aid interpretation of the results, we performed two additional simulations as a reference, identical to the cases above, but with the planet removed, i.e., considering the star with just the 5 G dipolar field, and with the CR2010 magnetogram.

In each simulation, the set of MHD equations is solved until convergence. The end result is a three-dimensional, steady-state solution for the particular system that includes all the MHD variables (density, pressure, velocity, and magnetic field). Since the MHD solution contains the values for n_e and T at each spatial cell, we can perform the line-of-sight integration to obtain the predicted X-ray emissions for a particular view angle. The integration takes into account cells in front of the star but omits cells behind it. We repeat this procedure for different view angles to mimic the predicted X-ray flux as the system rotates. The X-ray flux, f_x, is calculated as the line-of-sight integral $f_x \approx \int n_e^2 \cdot P(T) dl$. Here dl is the line-of-sight depth and we have used a piecewise linear approximation to the radiative loss $P(T)$ for a plasma with solar photospheric abundances (Giampapa et al. 1996).

3. RESULTS

Simulation results are illustrated in Figure 1. Top and middle panels show the three-dimensional solutions excluding and including the planet, respectively. Bottom panels show the difference in X-ray flux for temperature range of $\log(T) = 6.04$–6.23 with and without the planet. Left panels show results of Case A, while right panels show results of Case B.

Considering first Case A, we note a key difference between simulations with and without the planet. In the former, magnetic field lines are conspicuously brought in toward the planet and are constricted due to the presence of the planetary magnetosphere. This has a palpable influence on the coronal electron number density, n_e, which now increases azimuthally approaching the star–planet line to form an X-ray "bright spot" facing the planet. This solution is qualitatively very similar in Case B, where there is also a clear longitudinal concentration of the plasma density, and consequently the X-ray flux (which is proportional to n_e^2). While we cannot simulate chromospheric emission with our current models, its surface intensity distribution on the Sun follows closely those regions of the disk that are brighter at EUV and X-ray wavelengths. The results of these simulations are, then, fully consistent with the observed location of chromospheric hot spots seen in phase with the planetary orbit.

The longitudinal brightening effect is also clear in Figure 2, where the line-of-sight X-ray flux originating at different plasma temperatures is shown as a function of viewing angle for the simulations including planets. In the idealized dipole field case, the emission is much more intense when the corona is viewed from the direction of the planet than from the opposite direction when the star hides the brighter parts of the corona that form the hot spot in phase with the planet (a difference of 25%–35% in observed X-ray flux). The simulation based on the realistic, complex magnetic field results in a hot spot (15%–30% difference in X-ray flux) shifted by about 60° relative to the star–planet line. This suggests that the phase shifts between hot spots and planetary orbital phase seen in SPI observations are probably due to the complexity of the stellar coronal magnetic fields and the consequent complexity of the magnetic connectivity between the star and the planet.

Also of interest is the magnitude of the X-ray flux enhancement seen compared to the case where there is no planet. In the ideal dipole field case, we find enhancements of at least 10% in base emission and as much as ≈80% relative to the no-planet case, and a contrast between minimum and maximum of 20%–30%. These numbers are consistent with the observed signatures of SPI found in X-ray observations. When solutions driven by realistic magnetogram data are considered, we find that enhancements in base emission by a factor of 10 are possible. The simulation with realistic, complex magnetic field results in much higher density enhancement and closing of coronal loops compared to the dipolar case.

The MHD model, however, does not take into account the detailed physics of smaller scale X-ray emitting coronal loops,

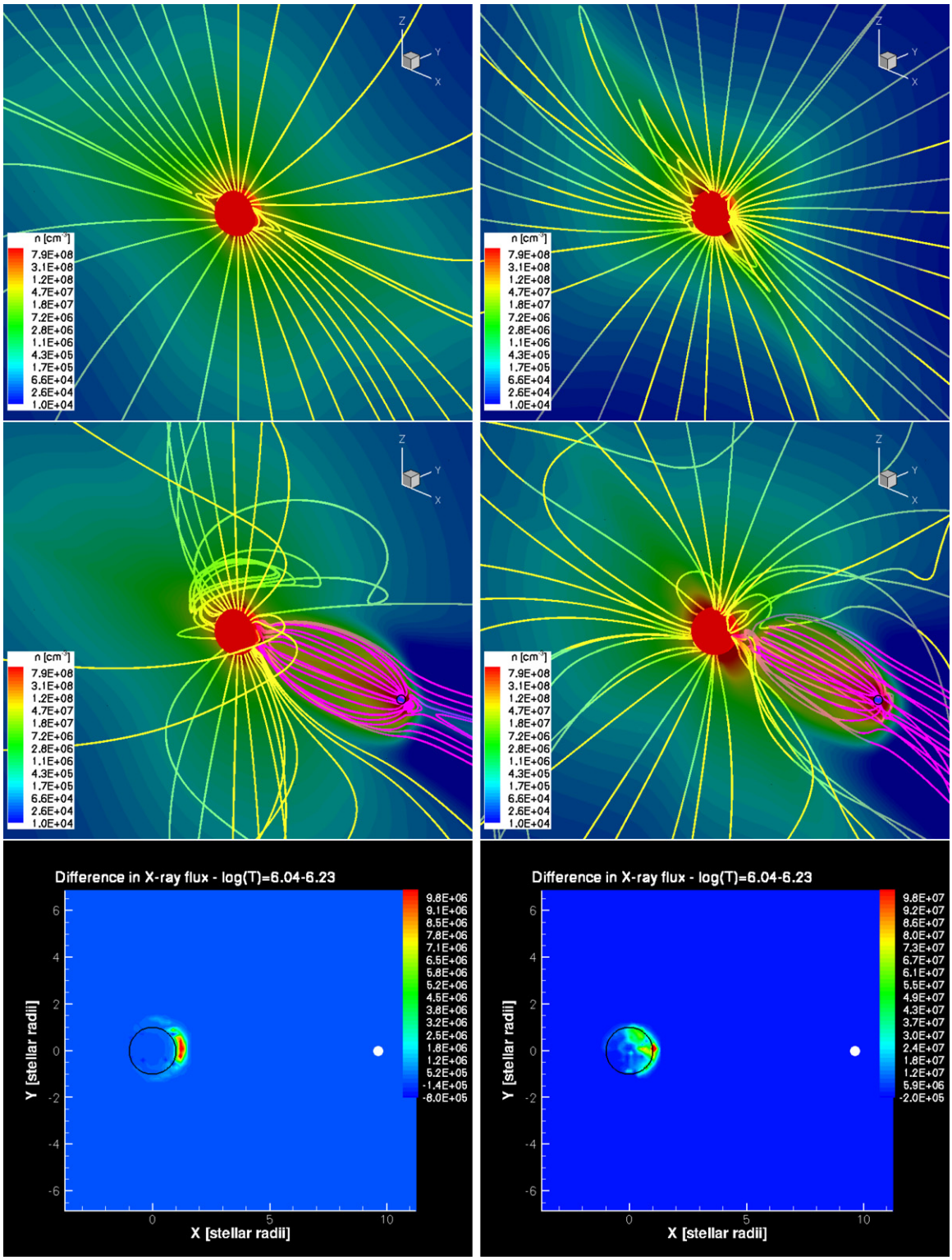

Figure 1. Illustration of the MHD simulation results for Case A (left), and Case B (right). The top panels show the reference simulations without the planet, while the simulations including the planet are shown in the middle panels (planetary surface is marked by black circle). Color contours represent plasma number density on the $y = 0$ plane, and yellow three-dimensional streamlines represent stellar magnetic field lines that originate on the intersection of the $y = 0$ plane with the stellar surface. The inner boundary of the simulation domain (the stellar surface) is represented by a red sphere, and the view is from an angle of 45°. In the middle panels, the magnetic field lines that connect to the planetary magnetosphere are drawn in pink. The bottom panels show the difference in X-ray emission for plasma in the logarithmic temperature range $\log T = 6.04$–6.23 between the case with and without the planet. Black circles represent the stellar surface and indicate that the "hot spots" are located in the low corona.

and the magnitude of the predicted X-ray enhancements should be considered approximate. The density enhancement in the closed-field zone provides a vital medium which can be heated to produce the SPI effect. The compression alone produces significant increase in radiative loss at low temperatures; localized dynamical effects, not modeled here, such as magnetic

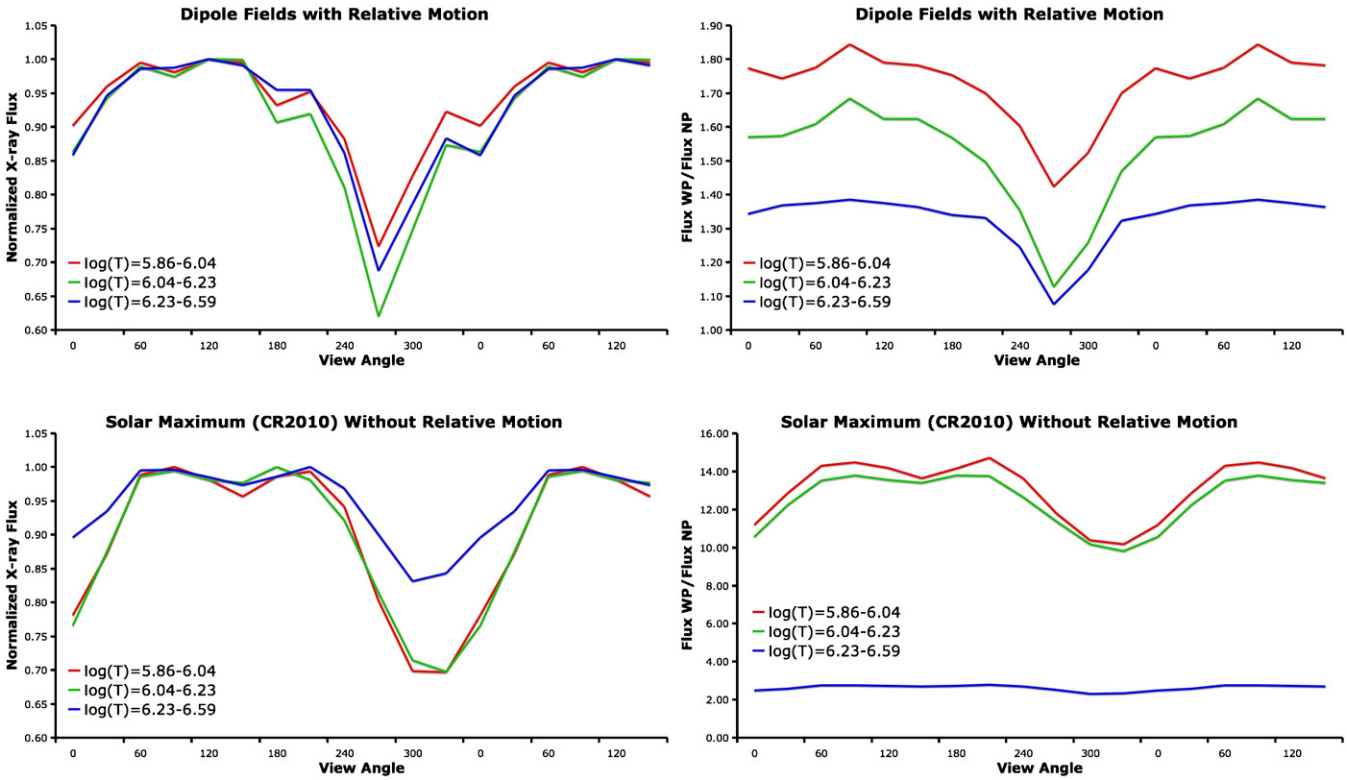

Figure 2. Integrated LOS X-ray flux for the dipolar case with relative orbital motion (top) and for the realistic solar maximum case (bottom) as a function of view angle. The planet is located at 90° and is hidden by the star at 270°. Left panels show the flux for three temperature bins, where each curve is normalized to its own maximum value. Right panels show the ratio of the X-ray flux with and without the planet for each temperature bin as a function of view angle.

reconnection due to the planetary orbital motion, and particle acceleration then likely further heat the plasma to the observed ∼1 keV temperatures (Saar et al. 2008).

4. CONCLUSIONS

In conclusion, we find that a dominant physical effect creating observable time-variable SPI signatures is that the existence of the planet and its magnetosphere, close to the star, prevents the expansion of the stellar coronal magnetic field and the acceleration of the stellar wind. The pressure gradient is not as large as it would be in the absence of the planet, so the coronal field lines that would be opened by the wind remain closed and the plasma in these loops does not escape. This effect alone reproduces three observable feature: (1) enhancement of total X-ray flux, (2) appearance of coronal hot spots, and (3) phase shift of the hot spots from the star–planet line. The density enhancement results in low-temperature coronal heating. We will further develop the model to include the planetary orbital motion in order to capture more dynamical effects of SPI.

This work has been inspired by an initial study performed by Noe Lugaz. We thank an unknown referee for his/her useful comments and Ruth Murray-Clay for useful discussion. O.C. is supported by NSF-SHINE ATM-0823592 grant, NASA-LWSTRT Grant NNG05GM44G. J.J.D. and V.L.K. were funded by NASA contract NAS8-39073 to the *Chandra X-ray Center*. Simulation results were obtained using the Space Weather Modelling Framework, developed by the Canter for Space Environment Modelling, at the University of Michigan with funding support from NASA ESS, NASA ESTO-CT, NSF KDI, and DoD MURI.

REFERENCES

Catala, C., Donati, J.-F., Shkolnik, E., Bohlender, D., & Alecian, E. 2007, MNRAS, 374, L42
Cohen, O., Sokolov, I. V., Roussev, I. I., & Gombosi, T. I. 2008, J. Geophys. Res. (Space Phys.), 113, 3104
Cohen, O., et al. 2007, ApJ, 654, L163
Cranmer, S. R., & Saar, S. H. 2007, arXiv:astro-ph/0702530
Cuntz, M., Saar, S. H., & Musielak, Z. E. 2000, ApJ, 533, L151
Giampapa, M. S., Rosner, R., Kashyap, V., Fleming, T. A., Schmitt, J. H. M. M., & Bookbinder, J. A. 1996, ApJ, 463, 707
Grießmeier, J.-M., et al. 2004, A&A, 425, 753
Kashyap, V. L., Drake, J. J., & Saar, S. H. 2008, ApJ, 687, 1339
Lanza, A. F. 2008, A&A, 487, 1163
Lanza, A. F. 2009, arXiv:0906.1738
Mayor, M., Naef, D., Pepe, F., Queloz, D., Santos, N., & Udry, S. 2003, The Geneva Extrasolar Planet Search Programmes, http://exoplanets.eu
Mayor, M., & Queloz, D. 1995, Nature, 378, 355
Murray-Clay, R. A., Chiang, E. I., & Murray, N. 2009, ApJ, 693, 23
Olson, P., & Christensen, U. R. 2006, Earth Planet. Sci. Lett., 250, 561
Powell, K. G., Roe, P. L., Linde, T. J., Gombosi, T. I., & de Zeeuw, D. L. 1999, J. Comput. Phys., 154, 284
Saar, S. H., Cuntz, M., Kashyap, V. L., & Hall, J. C. 2008, in IAU Symp. 249, Exoplanets: Detection, Formation and Dynamics, ed. Y.-S. Sun, S. Ferraz-Mello, & J.-L. Zhou (Dordrecht: Kluwer), 79
Saar, S. H., Cuntz, M., & Shkolnik, E. 2004, in IAU Symp. 219, Stars as Suns: Activity, Evolution and Planets, ed. A. K. Dupree & A. O. Benz (Dordrecht: Kluwer), 355
Sánchez-Lavega, A. 2004, ApJ, 609, L87
Shkolnik, E., Bohlender, D. A., Walker, G. A. H., & Collier Cameron, A. 2008, ApJ, 676, 628
Shkolnik, E., Walker, G. A. H., & Bohlender, D. A. 2003, ApJ, 597, 1092
Shkolnik, E., Walker, G. A. H., Bohlender, D. A., Gu, P.-G., & Kurster, M. 2005a, ApJ, 622, 1075
Shkolnik, E., Walker, G. A. H., Rucinski, S. M., Bohlender, D. A., & Davidge, T. J. 2005b, AJ, 130, 799
Tóth, G., et al. 2005, J. Geophys. Res. (Space Phys.), 110, 12226